coatings

MDPI

Article

Combustion Synthesis of UHTC Composites from Ti–B_4C Solid State Reaction with Addition of VIb Transition Metals

Chun-Liang Yeh * and Wei-Zuo Lin

Department of Aerospace and Systems Engineering, Feng Chia University, Taichung 40724, Taiwan; m0015856@fcu.edu.tw

* Correspondence: clyeh@fcu.edu.tw; Tel.: +886-4-2451-7250 (ext. 3963)

Academic Editors: Cheng Zhang, Arvind Agarwal and Kantesh Balani
Received: 10 May 2017; Accepted: 27 May 2017; Published: 1 June 2017

Abstract: UHTC composites were prepared by self-propagating high-temperature synthesis (SHS) from the Ti–B_4C reaction system with addition of Cr, Mo, and W. The starting sample composition was formulated as $(3-x)$Ti + B_4C + xMe with x = 0.1–1.0 and Me = Cr, Mo, or W. For all samples conducted in this study, self-sustaining combustion was well established and propagated with a distinct reaction front. With no addition of Cr, Mo, or W, solid state combustion of the 3Ti + B_4C sample featuring a combustion front temperature (T_c) of 1766 °C and a combustion wave velocity (V_f) of 16.5 mm/s was highly exothermic and produced an in situ composite of $2TiB_2$ + TiC. When Cr, Mo, or W was adopted to replace a portion of Ti, the reaction exothermicity was lowered, and hence, a significant decrease in T_c (from 1720 to 1390 °C) and V_f (from 16.1 to 3.9 mm/s) was observed. With addition of Cr, Mo, and W, the final products were CrB-, MoB-, and WB-added TiB_2–TiC composites. The absence of CrB_2, MoB_2, and WB_2 was attributed partly to the loss of boron from thermal decomposition of B_4C and partly to lack of sufficient reaction time inherent to the SHS process.

Keywords: self-propagating high-temperature synthesis (SHS); TiB_2–TiC composites; transition metal borides; B_4C; VIb transition metals

1. Introduction

Several borides and carbides of transition metals of the groups IVb and Vb are considered as ultra-high temperature ceramics (UHTCs) based on their melting temperatures in excess of 3000 °C and other properties, such as high hardness, high flexural strength, high thermal conductivity, and excellent resistance to thermal shock and corrosion [1–3]. UHTC composites—for example TiB_2–TiC, ZrB_2–SiC, ZrB_2–TaB_2, and NbB_2–SiC—have been of great importance for extreme environment applications requiring high thermal-shock resistance and durability against a rapid temperature change [4–7]. In addition, borides of chromium and tungsten have been recognized as effective reinforcements for UHTCs to improve densification, mechanical properties, and oxidation resistance [8,9].

Hot pressing (HP) and spark plasma sintering (SPS) are two most commonly-used fabrication routes to prepare UHTCs and composites on their basis [2–8]. Combustion synthesis in the mode of self-propagating high-temperature synthesis (SHS) has been a promising alternative, which takes advantage of highly exothermic reactions, and hence, has merits of low energy requirement, short processing time, simplicity, and high-purity products [10–12]. A number of borides and carbides of transition metals (mostly the groups IVb and Vb) have been produced by the SHS process from the elemental powder compacts of their corresponding stoichiometries [13–17]. Due to the low reaction enthalpy, however, solid state combustion between the transition metals of the group-VIb (Cr, Mo, and W) and boron or carbon is not feasible [12].

Of particular interest for this study is the TiB_2–TiC composite, because not only is it an outstanding UHTC [18,19], but it can also be produced through the SHS scheme with Ti and B_4C as the precursors [20–25]. The SHS process allows in situ synthesis of multi-phase materials, as in the case of TiB_2–TiC composites. The direct reaction of Ti with B_4C at stoichiometry of Ti:B_4C = 3:1 was sufficiently exothermic ($\Delta H = -686$ kJ/mol) to be self-sustaining and produced an in situ composite with TiB_2:TiC = 2:1 [20]. The exothermic mixture of 3Ti + B_4C has also been employed to fabricate TiB_2/TiC-based cermets with different metal binders such as Al, Cu, and Ni [21–23]. By combining a thermite reagent of CrO_3 + 2Al into the 3Ti + B_4C reaction system, Huang et al. [24] obtained TiB_2–TiC composites through combustion synthesis under an ultra-high gravity field which improved microstructure refinement, relative density, fracture toughness, and bending strength of the final products. Combustion synthesis of the TiC-rich composites with TiB_2:TiC = 1:2 and 1:4 was carried out in the Ti–B_4C–C reaction system [20,25]. Deorsola et al. [25] adopted carbon nanotubes in partial substitution for graphite in the sample of 6Ti + B_4C + 3C to facilitate the formation of nanostructured TiB_2–TiC composite powders.

The SHS method allows the formation of a variety of powders (including TiB_2, TiC, ZrB_2, ZrC, Cr_3C_2, TiN, NiAl, TiAl, FeAl, and $MoSi_2$) in size ranges and with an external morphology suitable as feedstock materials for different thermal spraying techniques [26]. Different kinds of plasma spraying (PS) methods [27,28], as well as detonation spraying (DS), flame spraying (FS), and high-velocity oxygen-fuel spraying (HVOF) are in common use for depositing protective coatings from SHS powders [26,29,30].

This study made the first attempt to explore in situ UHTC composites formed from the Ti–B_4C combustion system with addition of Cr, Mo, and W. As mentioned above, borides of the group-VIb metals were effective reinforcements for UHTCs, but they failed to be produced by the SHS method. Therefore, this study aimed to achieve simultaneous formation of borides of the group-VIb metals along with TiB_2 and TiC from the Ti–B_4C–Me (Me = Cr, Mo, and W) combustion systems. The phase composition of the SHS-derived products was examined. The influence of Cr, Mo, and W addition was investigated on combustion sustainability, flame-front velocity, and reaction temperature.

2. Materials and Methods

The starting materials adopted by this study included Ti (Alfa Aesar, Ward Hill, MA, USA, <45 μm, 99.5%), Cr (Alfa Aesar, <45 μm, 99.5%), Mo (Strem Chemicals, Newburyport, MA, USA, <45 μm, 99.9%), W (Alfa Aesar, <45 μm, 99.9%), and B_4C (Showa Chemical, Tokyo, Japan, <10 μm, 99.5%). The reactant mixtures were prepared based on a modification of the 3Ti + B_4C stoichiometry. The VIb group transition metal (Me = Cr, Mo, and W) was introduced to replace a portion of Ti, as expressed in Reaction (1).

$$(3 - x)\text{Ti} + B_4C + x\text{Me} \rightarrow (2 - x)TiB_2 + \text{TiC} + x\text{MeB} \quad (1)$$

where the stoichiometric coefficient, x, signifies the content of Cr, Mo, or W in the reactant mixture. The amounts of Cr, Mo, and W varying from x = 0.1–1.0 were considered. Because the reaction mechanism of simultaneous synthesis of TiB_2 and TiC is characterized firstly by the formation of TiC phase [18,31], the group-VIb metal added into the Ti–B_4C reaction system is supposed to react with boron and yield a boride compound denoted by MeB in Reaction (1).

The reactant powders were well mixed and compressed into cylindrical test specimens 7 mm in diameter, 12 mm in length, with a relative density of 55%. The SHS reaction was conducted under high-purity (99.99%) argon of 0.15 MPa. The ignition was accomplished by a heated tungsten coil with a voltage of 60 V and a current of 1.5 A. The combustion process was recorded by a color CCD video camera (Pulnix TMC-7, Babb, MT, USA) at 30 frames per second. The exposure time of each recorded image was set at 0.1 ms. The combustion wave velocity was determined from the time sequences of recorded images. To facilitate the accurate measurement of instantaneous locations of the combustion front, a beam splitter (Rolyn Optics, Covina, CA, USA), with a mirror characteristic of 75% transmission and 25% reflection, was used to optically superimpose a scale onto the image of the test

sample. The combustion temperature of the sample was measured by a fine-wire (125 μm) Pt/Pt-13% Rh thermocouple attached on the sample surface. The synthesized products were analyzed by an X-ray diffractometer (XRD) (Bruker, D8 SSS, Billerica, MA, USA) to identify the phase constituents. Details of the experimental methods were reported elsewhere [32].

3. Results and Discussion

3.1. Combustion Front Velocity and Combustion Temperature

Two typical combustion sequences illustrated in Figure 1a,b are associated with powder compacts of 2.5Ti + B_4C + 0.5Mo and 2.1Ti + B_4C + 0.9Cr, respectively. For either SHS process, a distinct combustion front formed upon ignition and propagated along the sample compact in a self-sustaining manner. It is evident that solid state combustion of Figure 1a is not only faster but more glowing than that of Figure 1b. This was caused by the fact that the formation enthalpy of MoB ($\Delta H_f = -123.9$ kJ/mol) is larger than that of CrB ($\Delta H_f = -78.9$ kJ/mol) [33]. As a result, the Mo-added sample is more energetic than the sample containing Cr. Besides, the content of Mo ($x = 0.5$) in the sample of Figure 1a is less than that of Cr ($x = 0.9$) in the sample of Figure 1b. To be presented later, the existence of TiB was found in the final products of Cr- and Mo-added samples and a larger amount of TiB was detected from the sample containing Mo. Because the formation of TiB ($\Delta H_f = -160.2$ kJ/mol) is very exothermic, the stronger combustion luminosity observed in Figure 1a might be due partly to the formation of more TiB. It should be noted that the addition of Cr, Mo, or W into the Ti–B_4C combustion system reduces the overall reaction exothermicity, since TiB_2 has a much larger formation enthalpy ($\Delta H_f = -315.9$ kJ/mol) than CrB, MoB, and WB [33]. As shown in Figure 1, the burned samples were slightly elongated. This resulted in the synthesized composites with a relative density of about 50–53%.

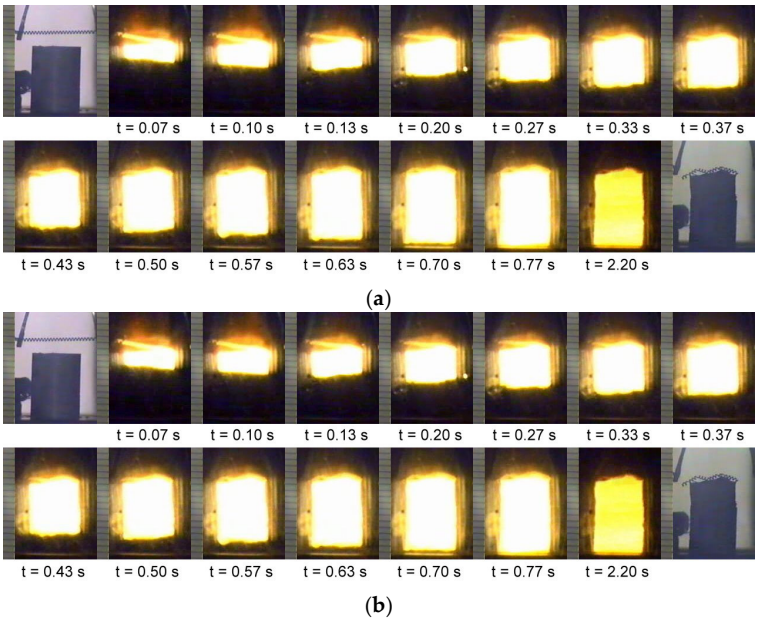

Figure 1. Time sequences of recorded images illustrating self-sustaining combustion propagating along powder compacts with stoichiometries of (**a**) 2.5Ti + B_4C + 0.5Mo and (**b**) 2.1Ti + B_4C + 0.9Cr.

Figure 2 presents the effect of Cr, Mo, and W addition on V_f of the sample. As can be seen in Figure 2, the flame-front velocity of the 3Ti + B_4C sample is as high as 16.5 mm/s but the flame velocity decreases significantly with increasing content of Cr, Mo, and W. This implies a dilution effect on combustion. Among three different Me-containing samples, the Mo-added sample exhibits the highest combustion wave velocity which decreases from 16.1 to 7.0 mm/s as the content of Mo increases from $x = 0.1$ to 1.0. For the other two types of samples with $x = 0.1$ to 1.0, the Cr-added sample has a higher

flame-front velocity descending from 15.9 to 4.6 mm/s, compared to a declining velocity from 15.6 to 3.9 mm/s for the W-added sample. The slow combustion wave observed for the W-added sample was attributed to the relatively low formation enthalpy of WB ($\Delta H_f = -66.1$ kJ/mol).

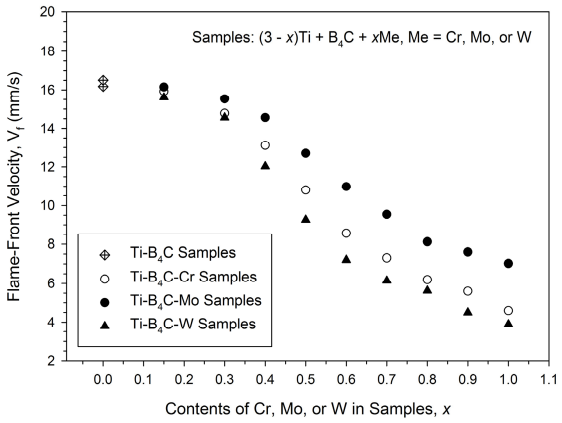

Figure 2. Variations of flame-front velocity with contents of Cr, Mo, and W added into Ti-B_4C samples.

Typical combustion temperature profiles of the powder compacts containing different amounts of Cr, Mo, and W are plotted in Figure 3. The abrupt rise in temperature signifies rapid arrival of the combustion wave and the peak value stands for the combustion front temperature. Profile #1 of Figure 3 is associated with the 3Ti + B_4C sample which shows a reaction front temperature reaching up to 1766 °C. Profiles #2 and #3, having their peak temperatures of 1684 and 1582 °C, were measured from Mo-added samples with x = 0.4 and 0.7, respectively. Temperature profiles (#4 and #5) of the Cr-added samples with x = 0.6 and 0.9 exhibited combustion front temperatures of 1511 and 1462 °C, respectively. In addition, the lowest reaction front temperature of about 1394 °C was observed in the W-added sample of 2Ti + B_4C + W (x = 1.0). In summary, the temperature measurement indicated that the addition of Cr, Mo, or W caused a decrease in the combustion front temperature that was further lowered as the amounts of Cr, Mo, and W increased. In agreement with the above observations, the Mo-added sample is the most exothermic while the W-containing sample is the least. The presence of TiB in the synthesized composites of Cr- and Mo-added samples could contribute partly to the findings that V_f and T_c of the Cr- and Mo-added samples are higher than those of the W-added samples. Moreover, the dependence of combustion temperature on sample stoichiometry is in a manner consistent with that of combustion wave velocity.

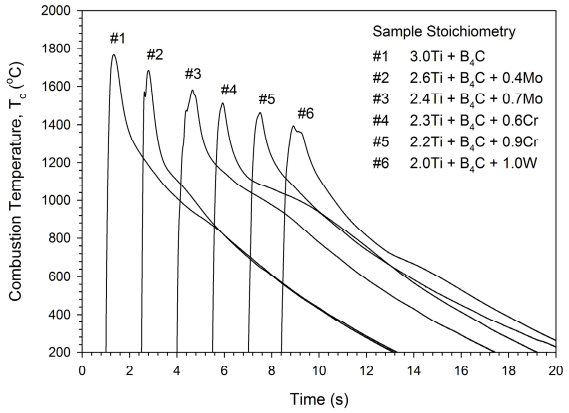

Figure 3. Combustion temperature profiles of Ti-B_4C samples added with different amounts of Cr, Mo, or W.

3.2. Phase Constituents of Synthesized Composites

The XRD pattern of Figure 4a indicates that phase constituents of the final product obtained from the 3Ti + B_4C sample consists of no more than TiB_2 (JCPDS 85-2083) and TiC (JCPDS 89-3828). This implies a complete conversion from the reactants to products. For the Cr-added sample of 2Ti + B_4C + Cr, Figure 4b shows the production of CrB (JCPDS 89-3587) and TiB (JCPDS 89-3922) in addition to TiB_2 and TiC. Formation of chromium monoboride (CrB) rather than diboride (CrB_2) suggests the possibility of loss of boron from thermal decomposition of B_4C during the SHS process. Because thermal dissociation of B_4C yielded gaseous boron [34], a small amount of $B_{(g)}$ escaped from the porous powder compact during the SHS process. This caused a loss of boron, which was also responsible for the presence of TiB.

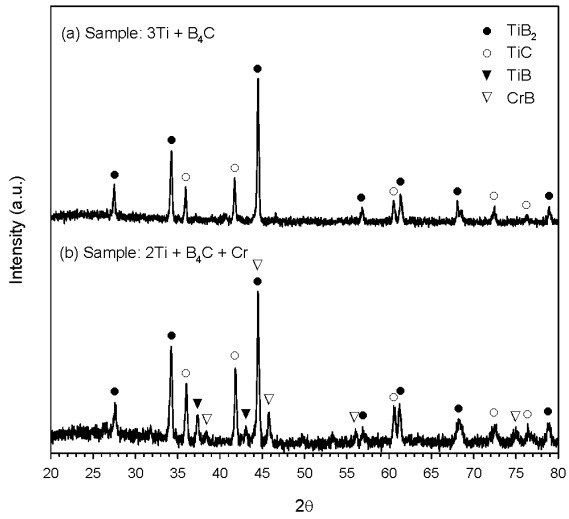

Figure 4. XRD patterns of SHS-derived composites from samples with stoichiomerties of (**a**) 3Ti + B_4C and (**b**) 2Ti + B_4C + Cr.

Figure 5a reveals that the composite synthesized from the Mo-added sample of 2Ti + B_4C + Mo is composed of TiB_2, TiC, TiB (JCPDS 73-2148), and MoB (JCPDS 06-0644). The presence of MoB and TiB was likely due to the loss of boron at the elevated temperatures. It should be noted that TiB of the cubic phase was formed in the final product of the Cr-added sample, while TiB of the orthorhombic phase was identified in the product of the Mo-added sample. The XRD signatures of TiB in Figures 4a and 5a correspond to their different phases.

When W was utilized as the substituent for a part of Ti, as shown in Figure 5b, the SHS-derived composite was a mixture of TiB_2, TiC, and WB (JCPDS 73-1769). It is noteworthy that monoborides (CrB, MoB, and WB) were produced from the Ti–B_4C system with additions of Cr, Mo, and W. The absence of diborides (CrB_2, MoB_2, and WB_2) might be also due to the lack of sufficient reaction time stemming from the fast combustion wave and rapid cooling rate inherent to the SHS process. This study demonstrated the production of Cr-, Mo-, and WB-added TiB_2–TiC composites by an energy- and time-saving fabrication route.

Figure 6a reveals the typical microstructure of fracture surface of the composite synthesized from the 3Ti + B_4C sample. The microstructure consisted of equiaxed TiC grains and TiB_2 platelets with an aspect ratio of about 2. For the Cr-added sample of 2Ti + B_4C + Cr, Figure 6b exhibits a granular morphology for its resultant composite which is a mixture of TiB_2, TiC, TiB, and CrB. Agglomeration of micro-sized grains is obvious. Figure 6c illustrates the microstructure of a WB-added TiB_2–TiC composite obtained from the W-added sample of 2Ti + B_4C + W. As can be seen in Figure 6c, TiB_2 platelets and TiC and WB grains are tightly aggregated. According to Figure 6a–c, it is suggested that

the morphologies of SHS-derived products from the Ti–B_4C samples with and without addition of Cr, Mo, and W have no substantial difference.

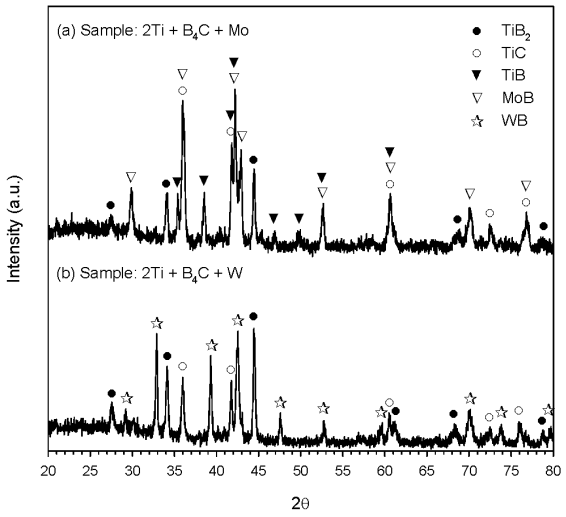

Figure 5. XRD patterns of SHS-derived composites from samples with stoichiomerties of (**a**) 2Ti + B_4C + Mo and (**b**) 2Ti + B_4C + W.

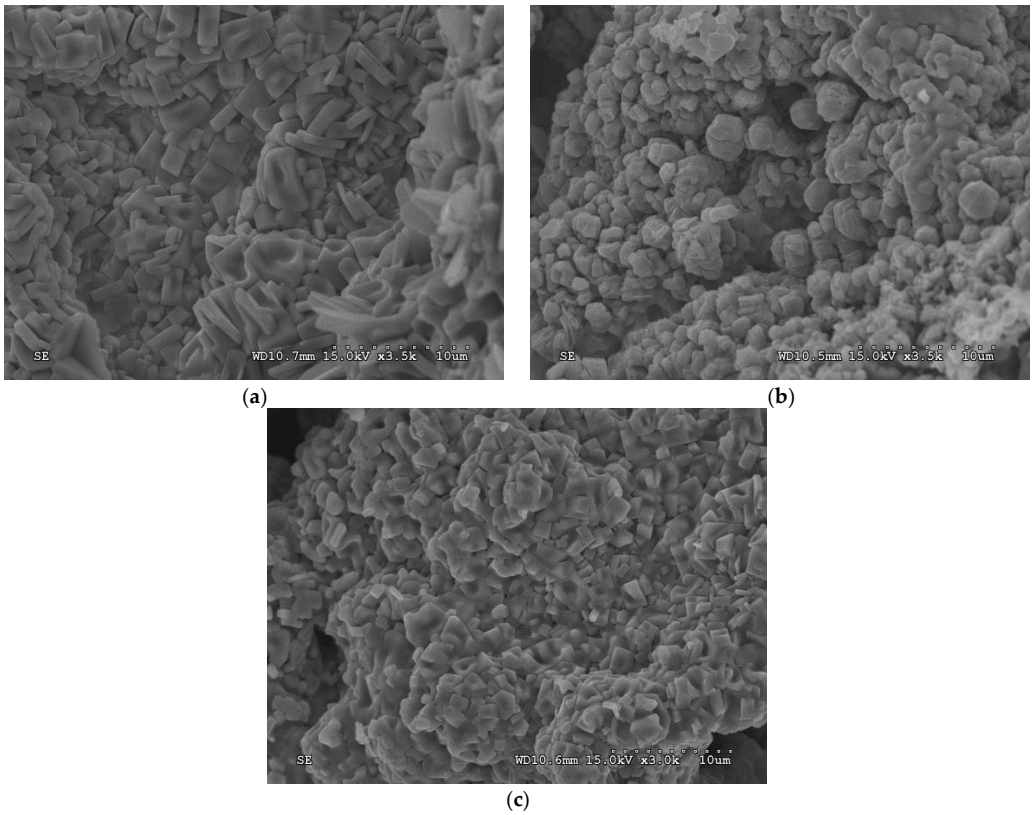

Figure 6. SEM micrographs of SHS-derived composites from samples with stoichiomerties of (**a**) 3Ti + B_4C, (**b**) 2Ti + B_4C + Cr, and (**c**) 2Ti + B_4C + W.

4. Conclusions

Fabrication of in situ UHTC composites from Cr-, Mo-, and W-added Ti–B_4C systems was studied by the SHS process. The reactant stoichiometry was designed as $(3-x)$Ti + B_4C + xMe with x = 0.1–1.0

and Me = Cr, Mo, or W. With no addition of Cr, Mo, and W, solid state combustion of the 3Ti + B_4C sample was highly exothermic and characterized by a reaction front temperature of 1766 °C and a combustion wave velocity of 16.5 mm/s. The product of the 3Ti + B_4C sample was a 2TiB_2 + TiC composite. When Cr, Mo, and W were adopted in partial substitution for Ti, the reaction exothermicity was reduced, thus leading to a considerable decrease in the combustion temperature and velocity. With the increase of Cr, Mo, and W from x = 0.1–1.0, the reaction front temperature decreased from about 1720 to 1390 °C and flame-front speed from 16.1 to 3.9 mm/s. Depending on the formation enthalpies of CrB, MoB, and WB, the Mo-added reaction is the most exothermic and the W-containing sample is the least. The XRD patterns showed that with the addition of Cr, Mo, and W, the final products contained CrB, MoB, and WB simultaneously formed along with TiB_2 and TiC. Besides, the presence of TiB was detected in the products of Cr- and Mo-added samples. Formation of monoborides (TiB, CrB, MoB, and WB) could be a consequence of the loss of boron at elevated temperatures and lack of sufficient reaction time for further phase transformation. In summary, the SHS process was shown to be an in situ fabrication route to preparing Cr-, Mo-, and WB-added TiB_2–TiC composites.

Acknowledgments: This research was sponsored by the Ministry of Science and Technology (Taiwan) under the grant of MOST 105-2221-E-035-039-MY2. Authors are grateful for the Precision Instrument Support Center of Feng Chia University in providing materials analytical facilities.

Author Contributions: Chun-Liang Yeh conceived and designed the experiments, analyzed the experimental data, supervised the work, and wrote the paper. Wei-Zuo Lin performed the SHS experiments and materials analysis.

Conflicts of Interest: The authors declare no conflict of interest. The founding sponsors had no role in the design of the study; in the collection, analyses, or interpretation of data; in the writing of the manuscript, or in the decision to publish the results.

References

1. Fahrenholtz, W.G.; Hilmas, G.E.; Talmy, I.G.; Zaykoski, J.A. Refractory diborides of zirconium and hafnium. *J. Am. Ceram. Soc.* **2007**, *90*, 1347–1364. [CrossRef]
2. Chakraborty, S.; Debnath, D.; Mallick, A.R.; Das, P.K. Mechanical and thermal properties of hot pressed ZrB_2 system with TiB_2. *Int. J. Refract. Met. Hard Mater.* **2014**, *46*, 35–42. [CrossRef]
3. Gürcan, K.; Ayas, E. In-situ synthesis and densification of HfB_2 ceramics by the spark plasma sintering technique. *Ceram. Int.* **2017**, *43*, 3547–3555. [CrossRef]
4. Wang, L.; Liu, H.; Huang, C.; Liu, X.; Zou, B.; Zhao, B. Microstructure and mechanical properties of TiC–TiB_2 composite cermet tool materials at ambient and elevated temperature. *Ceram. Int.* **2016**, *42*, 2717–2723. [CrossRef]
5. Guo, W.M.; Yang, Z.G.; Zhang, G.J. Comparison of ZrB_2–SiC ceramics with Yb_2O_3 additive prepared by hot pressing and spark plasma sintering. *Int. J. Refract. Met. Hard Mater.* **2011**, *29*, 452–455. [CrossRef]
6. Demirskyi, D.; Vasylkiv, O. Flexural strength behavior of a ZrB_2–TaB_2 composite consolidated by non-reactive spark plasma sintering at 2300 °C. *Int. J. Refract. Met. Hard Mater.* **2017**, *66*, 31–35. [CrossRef]
7. Demirskyi, D.; Vasylkiv, O. Mechanical properties of SiC–NbB_2 eutectic composites by in situ spark plasma sintering. *Ceram. Int.* **2016**, *42*, 19372–19385. [CrossRef]
8. Murthy, T.S.R.Ch.; Sonber, J.K.; Subramanian, C.; Fotedar, R.K.; Gonal, M.R.; Suri, A.K. Effect of CrB_2 addition on densification, properties and oxidation resistance of TiB_2. *Int. J. Refract. Met. Hard Mater.* **2009**, *27*, 976–984. [CrossRef]
9. Momozawa, A.; Telle, R. Controlled precipitation of W_2B_4 platelets and of β-WB nanolaminates for the in situ reinforcement of ternary TiB_2–W_2B_4–CrB_2 ceramics. *J. Eur. Ceram. Soc.* **2012**, *32*, 85–95. [CrossRef]
10. Merzhanov, A.G. Combustion and explosion processes in physical chemistry and technology of inorganic materials. *Russ. Chem. Rev.* **2003**, *72*, 289–310. [CrossRef]
11. Liu, G.; Li, J.; Chen, K. Combustion synthesis of refractory and hard materials: A review. *Int. J. Refract. Met. Hard Mater.* **2013**, *39*, 90–102. [CrossRef]
12. Yeh, C.L. Combustion synthesis: Principles and applications. In *Reference Module in Materials Science and Materials Engineering*; Hashmi., S., Ed.; Elsevier: Amsterdam, The Netherlands, 2016; pp. 1–8.

13. Radev, D.D.; Klissurski, D. Mechanochemical synthesis and SHS of diborides of titanium and zirconium. *J. Mater. Synth. Process.* **2001**, *9*, 131–136. [CrossRef]
14. Yeh, C.L.; Chen, W.H. A comparative study on combustion synthesis of Nb-B compounds. *J. Alloy. Compd.* **2006**, *422*, 78–85. [CrossRef]
15. Yeh, C.L.; Wang, H.J. A comparative study on combustion synthesis of Ta-B compounds. *Ceram. Int.* **2011**, *37*, 1569–1573. [CrossRef]
16. Dunmead, S.D.; Readey, D.W.; Semler, C.E.; Holt, J.B. Kinetics of combustion synthesis in the Ti-C and Ti-C-Ni systems. *J. Am. Ceram. Soc.* **1989**, *72*, 2318–2324. [CrossRef]
17. Yeh, C.L.; Liu, E.W. Combustion synthesis of tantalum carbides TaC and Ta_2C. *J. Alloy. Compd.* **2006**, *415*, 66–72. [CrossRef]
18. Vallauri, D.; Atías Adrián, I.C.; Chrysanthou, A. TiC-TiB_2 composites: A review of phase relationships, processing and properties. *J. Eur. Ceram. Soc.* **2008**, *28*, 1697–1713. [CrossRef]
19. Wang, D.; Wang, H.; Sun, S.; Zhu, X.; Tu, G. Fabrication and characterization of TiB_2/TiC composites. *Int. J. Refract. Met. Hard Mater.* **2014**, *45*, 95–101. [CrossRef]
20. Yeh, C.L.; Chen, Y.L. Combustion synthesis of TiC-TiB_2 composites. *J. Alloy. Compd.* **2008**, *463*, 373–377. [CrossRef]
21. Shen, P.; Zou, B.; Jin, S.; Jiang, Q. Reaction mechanism in self-propagating high temperature synthesis of TiC-TiB_2/Al composites from an Al-Ti-B_4C system. *Mater. Sci. Eng. A* **2007**, *454–455*, 300–309. [CrossRef]
22. Liang, Y.H.; Wang, H.Y.; Yang, Y.F.; Zhao, R.Y.; Jiang, Q.C. Effect of Cu content on the reaction behaviors of self-propagating high-temperature synthesis in Cu-Ti-B_4C system. *J. Alloy. Compd.* **2008**, *462*, 113–118. [CrossRef]
23. Yang, Y.F.; Wang, H.Y.; Zhao, R.Y.; Liang, Y.H.; Jiang, Q.C. Effect of Ni content on the reaction behaviors of self-propagating high-temperature synthesis in the Al-Ti-B_4C system. *Int. J. Refract. Met. Hard Mater.* **2008**, *26*, 77–83. [CrossRef]
24. Huang, X.; Zhao, Z.; Zhang, L.; Wu, J. The effects of ultra-high-gravity field on phase transformation and microstructure evolution of the TiC-TiB_2 ceramics fabricated by combustion synthesis. *Int. J. Refract. Met. Hard Mater.* **2014**, *43*, 1–6. [CrossRef]
25. Deorsola, F.A.; Atias Adrian, I.C.; Ortigoza Villalba, G.A.; DeBenedatti, B. Nanostructured TiC-TiB_2 composites obtained by adding carbon nanotubes into the self-propagating high-temperature synthesis process. *Mater. Res. Bull.* **2011**, *46*, 995–999. [CrossRef]
26. Talako, T.; Ilyuschenko, A.; Letsko, A. SHS powders for thermal spray coating. *KONA Powder Part. J.* **2009**, *27*, 55–72. [CrossRef]
27. Licheri, R.; Orrù, R.; Cao, G.; Crippa, A.; Scholz, R. Self-propagating combustion synthesis and plasma spraying deposition of TiC-Fe powders. *Ceram. Int.* **2003**, *29*, 519–526. [CrossRef]
28. Xu, J.; Zou, B.; Zhao, S.; Hui, Y.; Huang, W.; Zhou, X.; Wang, Y.; Cai, X.; Cao, X. Fabrication and properties of ZrC–ZrB_2/Ni cermet coatings on a magnesium alloy by atmospheric plasma spraying of SHS powders. *Ceram. Int.* **2014**, *40*, 15537–15544. [CrossRef]
29. Xanthopoulou, G.; Marinou, A.; Vekinis, G.; Lekatou, A.; Vardavoulias, M. Ni-Al and NiO-Al composite coatings by combustion-assisted flame spraying. *Coatings* **2014**, *4*, 231–252. [CrossRef]
30. Xanthopoulou, G.; Marinou, A.; Karanasios, K.; Vekinis, G. Combustion synthesis during flame spraying ("CAFSY") for the production of catalysts on substrates. *Coatings* **2017**, *7*, 14. [CrossRef]
31. Contreras, L.; Turrillas, X.; Vaughan, G.B.M.; Kvick, Å.; Rodríguez, M.A. Time-resolved XRD study of TiC-TiB_2 composites obtained by SHS. *Acta Mater.* **2004**, *52*, 4783–4790. [CrossRef]
32. Yeh, C.L.; Chen, Y.L. An experimental study on self-propagating high-temperature synthesis in the Ta-B_4C system. *J. Alloy Compd.* **2009**, *478*, 163–167. [CrossRef]
33. Binnewies, M.; Milke, E. *Thermochemical Data of Elements and Compounds*; Wiley-VCH Verlag GmbH: Weinheim, NY, USA, 2002.
34. Hildenbrand, D.L.; Hall, W.F. The decomposition pressure of boron carbide and the heat of sublimation of boron. *J. Phys. Chem.* **1964**, *68*, 989–993. [CrossRef]